International Journal of Concrete Structures and Materials

RESEARCH

Open Access

# Investigation on Acoustic Emission Parameters due to Fatigue Damage of Concrete Beams with Variable Notched Depth

Sakhiah Abdul Kudus[1,2*], Norazura Muhamad Bunnori[3], Nur Kamaliah Mustaffa[1] and Adiza Jamadin[1,2]

**Abstract**

Acoustic Emission (AE) application for Structural Health Monitoring (SHM) has undergone a swift advance through research and innovation in recent times. The AE monitoring is widely exploited as a tool for damage detection in materials research and structure monitoring. Various advantages of the AE, such as the potential use in large and complex structures, high-sensitivity, real-time monitoring capability, and potential application across a wide range of field study, has given the technique an edge over other approaches. Nevertheless, most of the reported studies had focused on the interpretation of the results in both quantitative and qualitative perspectives to extend the capabilities and application of AE for damage detection strategy. Eventually, the quantification of the damage level of the concrete structure relative to fatigue loading remained unanswered. Therefore, this study presented the experimental investigation of four types of plain concrete beams with a fixed dimension of 100 × 200 × 600 mm in the different notch-to-depth ratios under cyclic loading. A setup of the instrument consisting of four AE sensors type R6I was employed on each concrete beam sample to ensure a precise measurement for the three-point bending test. The *b*-value, improved *b*-value (Ib-value), severity, and intensity analysis methods were applied to quantify the damage level of the concrete structure under fatigue loading. Based on the results, the AE analysis successfully classified the damage levels following the observation made during the increasing cyclic loading on the notched concrete beams, the initiation of cracks, the steady growth of cracks, and beam failure. Valuable insights were recorded throughout the observation, including the progression of the fatigue failure mechanism from the Ib-value results, the intensity chart patterns from the intensity analysis, and the increased severity due to the increased loading cycles from the severity analysis. Conclusively, this study would enable researchers to understand the trend in monitoring the damage level under fatigue loading using the AE technique as well as providing fresh insights for further research.

**Keywords:** acoustic emission, *b*-value, Ib-value, severity, intensity, concrete, fatigue

## 1 Introduction

The rising concern over structural deterioration and structural failures has taken centre stage as ageing structures gradually deteriorates and poses a potential hazard. The failures have been attributed to many factors, including the increase in loading, severe environmental pollution, improper construction methods, and the lack of knowledge for maintenance. Various infrastructures, such as bridges, highways, and marine structures, are always subjected to cyclic fatigue loadings. Fatigue is the progressive process of permanent internal structural change due to repetitive loading. The prolonged process may result in structural fatigue failure as the fatigue loading could significantly affect the stiffness, toughness, and durability of the structures. In view of this, researchers have exploited a broad range of inspection methods for early detection and warning of potential critical defects.

*Correspondence: sakhiah@uitm.edu.my
[1] School of Civil Engineering, College of Engineering, Universiti Teknologi MARA, 40450 Shah Alam, Selangor, Malaysia
Full list of author information is available at the end of the article
Journal information: ISSN 1976-0485 / eISSN2234-1315

Springer Open

© The Author(s) 2022. **Open Access** This article is licensed under a Creative Commons Attribution 4.0 International License, which permits use, sharing, adaptation, distribution and reproduction in any medium or format, as long as you give appropriate credit to the original author(s) and the source, provide a link to the Creative Commons licence, and indicate if changes were made. The images or other third party material in this article are included in the article's Creative Commons licence, unless indicated otherwise in a credit line to the material. If material is not included in the article's Creative Commons licence and your intended use is not permitted by statutory regulation or exceeds the permitted use, you will need to obtain permission directly from the copyright holder. To view a copy of this licence, visit http://creativecommons.org/licenses/by/4.0/.

Fatigue failure is a well-known condition in metals. Despite the characteristics and quality of metals are strictly maintained throughout the manufacturing process, the mechanism of concrete's fatigue properties is less comprehended owing to the material's heterogeneous microstructure. Additionally, concretes have a weak point, including voids of various sizes, pre-existing micro-cracks in aggregates, and a limited bonds between the aggregate and matrix, which might facilitates the formation of a crack.

Realising the essential need to monitor and assess any damage to aid maintenance strategies and provide an accurate prediction of the remaining lifespan, various techniques have been developed for damage assessment. One of the common techniques is the powerful and non-destructive Structural Health Monitoring (SHM) that evaluates and quantify the damage and further ensure the safety and reliability of the infrastructure in civil engineering. In recent years, SHM has been increasingly applied via several approaches in multiple literature, including smart sensor and wireless (Lynch et al., 2006; Kim et al., 2006; Lynch, 2007; Nagayama and Spencer, 2007); machine learning (Worden and Manson, 2007; Farrar and Worden, 2012; Yuan et al., 2020), fibre optic methods (Glišić and Inaudi, 2007; López-Higuera et al., 2011), guided wave (Raghavan, 2007; Croxford et al., 2007; Mitra and Gopalakrishnan, 2016), and Global Positioning System (GPS) (Im et al., 2013). Since its inception in the early 1990s, SHM has been the subject of extensive research, with an emphasis on its ability to effectively monitor crack propagation and classification.

Meanwhile, the Acoustic Emission (AE) technique is emerging as a well-known non-destructive evaluation approach in SHM. AE differs from other techniques in that it is based on the analysis of elastic waves that are generated from material damage, such as the crack growth under cyclic loads. Additionally, AE is able to detect the dynamic process via the movement or strain, whereas most of the other non-destructive testing (NDT) methods could only detect existing geometrical discontinuities or fractures (Degala et al., 2009). For instance, Yuyama et al. (2001) used AE in the corner of a reinforced concrete rigid frame. This unique monitoring mechanism distinguishes itself from other non-destructive test methods, providing real-time information on the condition of damaged structures (Kurz, 2006). Besides that, the AE technique is capable of detecting various types of damages, such as fatigue cracks growth, corrosions, and delamination. Most studies on the AE technique have focused on crack location (Bunnori et al., 2011; Shiotani et al., 1999), quantifying the degree of damage (Proverbio, 2011; Degala et al., 2009; Lovejoy et al., 2008), determining the crack classification in concrete structures (Ohno et al., 2010; Aggelis et al., 2011), and investigate AE activities of steel reinforcements in reinforced concrete beams (Prashanth et al., 2019). Carpinteri et al. (2016) summarise that the type of cracks can be identified according to the AE parameters based characteristics of the fracture energy and the acoustic emission energy of the fracture surface from three-point bending (TPB) tests on notched concrete. Lacidogna et al. (2020) performed AE-based damage detection on concrete beams and attained the laws of fracture energy, bending strength, and AE energy.

Additionally, Prashanth et al. (2019) implied that the AE can be used to identify crack propagation in strengthened concrete beams through recognising bi-linear behaviours associated with mode crack propagation with adjustments in slopes on plots of AE occurrences and absolute AE energy with time as a feature of the number of fatigue loading cycles.

Although various investigations related to fatigue and AE have been performed, studies on the fatigue damage of concrete beams based on AE parameters remains limited. Therefore, this study aimed to investigate the fatigue damage of concrete beams using the AE technique under increasing fatigue amplitude. The quantification of this damage accumulation was needed to translate it into levels of deterioration. The *b*-value analysis, Ib-value analysis, severity analysis, and intensity analysis were applied in this study to indicate the level of deterioration and reliability of the concrete structures. The signal-based approach analysis was also employed to evaluate the damage detection.

## 2 AE Analysis

The main challenge of AE testing for damage assessment is the interpretation of the recorded AE data. Despite that the AE quantification is carried out based on the waveform analysis, a wide range of quantitative analysis techniques are available to be applied using the AE parametric data. The AE technique has been proven as an effective technique for local (Colombo et al., 2003), global (Holford et al., 2001), and continuous monitoring. Global monitoring provides users with the structural integrity of the whole structure, while local monitoring assesses the specific interest area. The AE technique exhibits high sensitivity and can detect crack growth at very early stages. In fact, Finlayson et al. (2001) reported that AE was found to be sufficiently sensitive to detect newly formed crack surfaces down to a few hundred square micrometres and less.

### 2.1 b-value Analysis

Material deterioration is frequently quantified using the b-value approach. The b-value is determined utilising seismology algorithms using the AE amplitude distribution data (Rao et al., 2005). In general, the b-value is defined as the logarithmic slope of AE's frequency magnitude distribution (Colombo et al., 2003). Gutenberg Richter proposed this magnitude-relationship, which can be derived using the following equation:

$$\log_{10} N = a - bM_{\mathrm{L}}, \tag{1}$$

where $M_{\mathrm{L}}$ = Richter magnitude of the events; $N$ = incremental frequency (the number of events with magnitudes in the range of $M_{\mathrm{L}} \pm \Delta M/2$); and $a$ and $b$ = empirical constants (Rao and Lakshmi, 2005; Colombo et al., 2003; Sagar et al., 2012). A similar principle can be applied to the AE method to study the generated AE wave during the cracking or fracture process of structures. However, in terms of AE technique, the Gutenberg–Richter formula is modified and represented by:

$$\log_{10} N = a - b(A_{\mathrm{dB}}/20), \tag{2}$$

where $N$ = incremental frequency; $A_{\mathrm{dB}}$ = peak amplitude of the AE events in decibels; $A_{\mathrm{dB}}/20$ = magnitude (M); $a$ = empirical constants; and $b$ = AE-based $b$-value. According to Colombo et al. (2003), in associating the cracking process, the initial micro-cracking generates many low amplitude AE signals, while the subsequent macro-cracking generates fewer signals with higher amplitude. This implies that the $b$-value decreased as the specimen approaches imminent failure or the slope decreased when the damage is more localised, as summarised in Table 1.

### 2.2 Ib-value Analysis

A variety of AE analyses have been reported in the literature. Given that the distribution of frequency versus amplitude of AE is not always linear, the b-value analysis method has been modified using certain statistical values of the amplitude distribution as the mean and standard deviation. This newer method is referred to as the Improved $b$-value (Ib-value) (Carpinteri et al., 2009). The Ib-value is expressed in Eq. (3) and Eq. (4):

**Table 1** The $b$-value quantitative results (Colombo et al., 2003).

| Range | Description |
|---|---|
| 1.0 < $b$-value < 1.2 | Micro-crack dominant |
| 1.2 < $b$-value < 1.7 | Macro-crack constant |
| $b$-value > 1.7 | Macro-crack opening |

$$\mathrm{Ib} = \frac{\log_{10} N(\omega_1) - \log_{10} N(\omega_2)}{(\alpha_1 + \alpha_2)\sigma}, \tag{3}$$

$$\omega_1 = \mu - \alpha_1\sigma, \omega_2 = \mu + \alpha_2\sigma, \tag{4}$$

where $N(\omega_1)$ is the accumulated number of AE events in which the amplitude is more than $\mu - \alpha_1\sigma$; $N(\omega_2)$ is the accumulated number of AE events, where the amplitude is more than $\mu + \alpha_2\sigma$; $\mu$ is the mean amplitude; $\sigma$ is the standard deviation of the amplitude distribution; and $\alpha_1$ and $\alpha_2$ are constants. The analysis is performed using groups formed by a number of events or hits. A group of 75 events was used by Kaphle et al. (2011), while a group of 100 events was used by Proverbio et al. (2009) and Angelis et al. (2009) in their studies.

### 2.3 Intensity Analysis

The intensity analysis is a technique that facilitates the evaluation of the overall structural integrity and structural significance of an AE event as well the level of deterioration of a structure by calculating two parametric values comprising the Historic Index (HI) and Severity ($S_{\mathrm{r}}$) (Golaski et al., 2002). Both the HI and $S_{\mathrm{r}}$ are modified parameters of AE and are considered as signal strength, which is an AE parameter that combines both amplitude and duration.

According to Gostautas et al. (2005), HI is an analytical approach for measuring the variations in the slope of the cumulative signal strength over time by comparing the signal strength of the most recent hits to the total signal strength for that channel. HI is used to determine the rate at which the signal strength changes during a test (ASTM E 2478, 2006). Occasionally, the HI is utilised to detect the onset of significant AE. Additionally, the HI is applied to measure the angle of the AE knee in the time-dependent cumulative signal strength curve. The AE knee is defined as the point on the line when the slope changes dramatically, resulting in an abrupt increase in the HI.

Meanwhile, $S_{\mathrm{r}}$ is defined as the average empirically derived constant based on the material ($J$), which signifies the largest signal strength emission (Degala et al., 2009). As the $S_{\mathrm{r}}$ is a measure of the structural damage, an increase in $S_{\mathrm{r}}$ often corresponds to new structural damage. Eventually, a significant increase of $S_{\mathrm{r}}$ occurs as the damage becomes more serious (Gostautas et al., 2005). The HI and $S_{\mathrm{r}}$ are defined by Eq. (5) and Eq. (6) (Golaski et al., 2002; Gostautas et al., 2005; Degala et al., 2009; Nair and Cai, 2010):

$$\mathrm{HI} = \frac{N}{N-K} \cdot \left( \frac{\sum_{i=K+1}^{N} S_{oi}}{\sum_{i=1}^{N} S_{oi}} \right), \tag{5}$$

$$S_r = \frac{1}{J} \times \left( \sum_{m=1}^{J} S_{om} \right), \quad (6)$$

where HI = historic index; $N$ = number of hits up to time $t$; $S_{oi}$ = signal strength of the $i$th hit; $S_r$ = severity index; $J$ = empirically derived constant based on the material; and $S_{om}$ = signal strength of the $m$th hit, where the order of $m$ is based on the magnitude of the signal strength. The relationship between $N$ and $K$ and $J$ values for the concrete were as follows:

$$K = 0, N \leq 50,$$

$$K = 0.8N, 101 \leq N \leq 500,$$

$$K = N - 100, N \geq 500,$$

$$J = 0, N < 20,$$

$$J = 20, N \geq 20.$$

An intensity chart is composed of the $S_r$ and maximum HI values, as shown in Fig. 1. The structural significance of the emission is indicated by different intensity levels, which is described in detail in Table 2. The chart is divided into intensity zones which indicate the structural significance of the emission. The signal strength is an effective parameter to describe the trend of AE data because it takes into account both the amplitude and duration (Chotickai, 2001). High signal strength is usually related to the damage development in a structure.

## 3 Experimental Procedure

### 3.1 Samples Preparation

The design of the beams followed the British Standard (BS) 8110:Part 1:1985 with a standard width, length, and height of 100 mm, 600 mm, and 200 mm, respectively. The concrete mixture was composed of Portland cement, water, river sand as fine aggregate, and crushed stones as coarse aggregate with a proportion of 1.00:0.46:1.40:3.26, respectively. The water-to-cement ($w/c$) ratio used for the concrete specimen was 0.47. The concrete beam was cast in the form of a flashboard for sample production. The vibrator was used during the casting for compacting purposes. The formwork was removed after 24 h and water cured for 60 days. After the curing process, the notched-on beam was made using a table saw cutting machine.

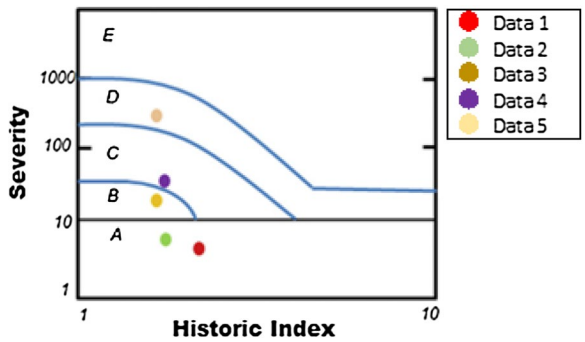


**Fig. 1** A typical intensity chart for concrete materials comprising the $S_r$ and HI (Degala et al., 2009).

**Table 2** Significant of intensity zones (Gostautas et al., 2005).

| Level | Recommended action |
|---|---|
| A[a] | Insignificant AE |
| B[b] | Note for reference in future tests. Typically minor surface defects, such as corrosion, pitting, gouges, or crack attachments welds |
| C | Defects requiring follow-up evaluation, which may be based on further data analysis or complementary non-destructive examination |
| D | Significant defect requiring follow-up inspection |
| E | Major defect requiring immediate shut-down and follow-up inspection |

[a] No significant emission.

[b] Minor.

All sizes specified for the beam tested followed the requirement of The International Union of Laboratories and Experts in Construction Materials, Systems, and Structures (RILEM) (1991). The maximum span-to-depth ratio allowed was 4, while the width size of the notch was based on the aggregate size used in the concrete specimen. The 20 mm aggregates size was fixed throughout the test and the size of width allowed was equal to 50% of the size of the aggregate, which corresponded to 10 mm (Kudus, 2014).

The specimens tested exhibit the same shape and size with the different notch-to-depth ratios for each type of beam. A total of four different types of notch-to-depth ratios were studied, cited as Type I (notch-to-depth ratio 0.15), Type II (notch-to-depth ratio 0.25), Type III (notch-to-depth ratio 0.35), and Type IV (notch-to-depth ratio 0.45). For each category, seven specimens were prepared. Four specimens were used for the variable amplitude test, and three samples for the static test. The shape and size of specimens with different notched lengths were kept the same.

The surface of all specimens was ground to ensure the notched beams have a smooth surface as the smoothness is important for even loading during the test. The static test was performed in a closed-loop controlled machine, Instron with a 250 kN load capacity, which was capable of testing large beams. A similar machine

was used to run the fatigue test. The flexural load was increased under displacement control at a rate of 0.003 mm/s each test.

### 3.2 Loading and AE System

The fatigue tests of the plain notched concrete beams under constant increasing amplitude of cyclic loads were carried out and the damage mechanism was analysed based on the AE data parameter and AE analysis. The SAX single-axis fatigue software was used to define and run the tests. Before the tests were performed, several parameters consisting of amplitude and mean level were first specified. These values were based on the maximum and minimum stress load. The AEwin software was used to analyse the collected data during the tests. AEwin software allows the user to replay the test's data.

The AE instrumentation consists of the transducers (sensors), pre-amplifiers, filters, amplifiers, and analysis software. The micro-SAMOS (μ-SAMOS) hardware was used throughout the experiment. The multichannel AE systems were needed to cover the entire area of the testing beam structure and obtain an accurate AE location. The use of grease couplant was necessary for the detection of low-level acoustic signals. The RG 58 cables were also used throughout the test due to their sturdiness with the Bayonet Neill–Concelman (BNC) connectors. A total of four AE sensors type R6I were used on each beam. Two sensors were placed on the side of the specimen, while the other two sensors were placed on top of the specimen, as indicated in Fig. 2. The four sensors were used to increase the accuracy of data and minimise data loss. The positioning of the sensors was crucial before the AE investigation was performed as poor sensor mounting would reduce the sensitivity of the detection and lead to a loss of significant AE data. The complete setup is shown in Fig. 3.

For the waveform setup, the sample rate was set to 100 kSPS, and the pre-trigger was set to 250 kSPS. The value of Peak Definition Time (PDT), Hit Definition Time (HDT), and Hit Lockout Time (HLT) were set to 500 microseconds, 1000 microseconds, and 500 microseconds, respectively. The HDT, PDT, and HLT were all timing parameters of the signal acquisition process and have material-specific values.

## 4 Results and Discussion

### 4.1 Static Test

The static test was conducted to identify the failure load of the specimen, which was correlated to the maximum load that can be sustained by each type of notched beam. The maximum or ultimate load was an essential parameter to predict the failure load of the specimen during testing. The purpose of a centred notch was to ensure that the first crack occurs at the narrow zone area, which was closer to the notch, where micro-crack appears and then links up to form macro-cracks. The notched specimen was also reported to provide a stable crack growth in previous studies (Karihaloo, 1995). According to the static load results in Table 3, the shortest depth of notch required a high load for failure, while the highest depth of notch required a small load for failure. This was because the notch resembles a pre-cracked specimen. As the notch-to-depth ratio increased, the brittleness of the beam decreased. Hence, the Type I beam was more brittle compared to the Type IV beam.

### 4.2 Parametric AE Data from Fatigue Test

The fatigue test was performed using samples at the age of 60 days instead of the usual age testing of 28 days to minimise the strength gained due to ageing during the test. A 1.0 Hz frequency of sinusoidal cyclic loading was constantly applied on all specimens tested under the fatigue test. The fatigue loading was applied in a

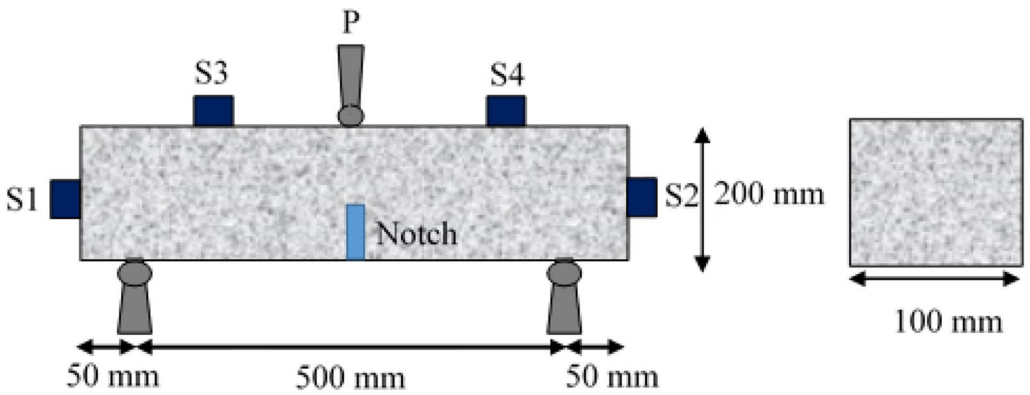


**Fig. 2** Setup of the instrument for three-point bending test.

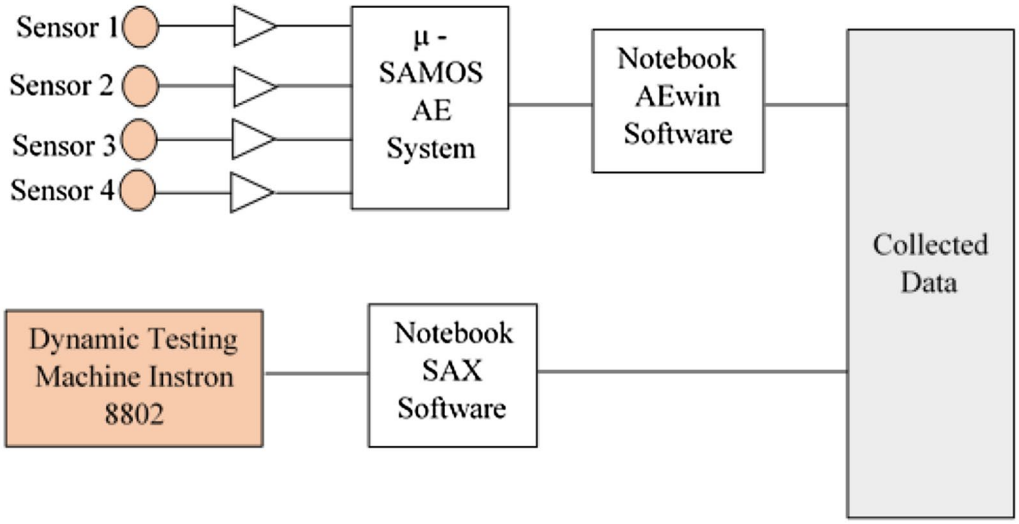


**Fig. 3** Complete schematic diagram of the connection setup.

**Table 3** Maximum static load for each type of specimen.

| Specimen | Ultimate load, $P_{ult}$ (kN) | | | Average $P_{ult}$ (kN) |
|---|---|---|---|---|
| | Beam 1 | Beam 2 | Beam 3 | |
| Type I | 16.91 | 15.99 | 15.10 | 16.00 |
| Type II | 8.31 | 14.01 | 10.68 | 11.00 |
| Type III | 9.37 | 9.11 | 8.52 | 9.00 |
| Type IV | 5.79 | 6.16 | 5.45 | 5.80 |

step-wise increase of loading, where the maximum loading was increased by 0.5 kN for each load stage that contains 250 cyclic loadings. The minimum load limit was kept constant at 0.2 kN for all cycles and all specimens' types. The minimum load was used to avoid the impact loading during the application of the cyclic load as well as allowing the measure of unloading compliance so that the system has some contact between the specimen and

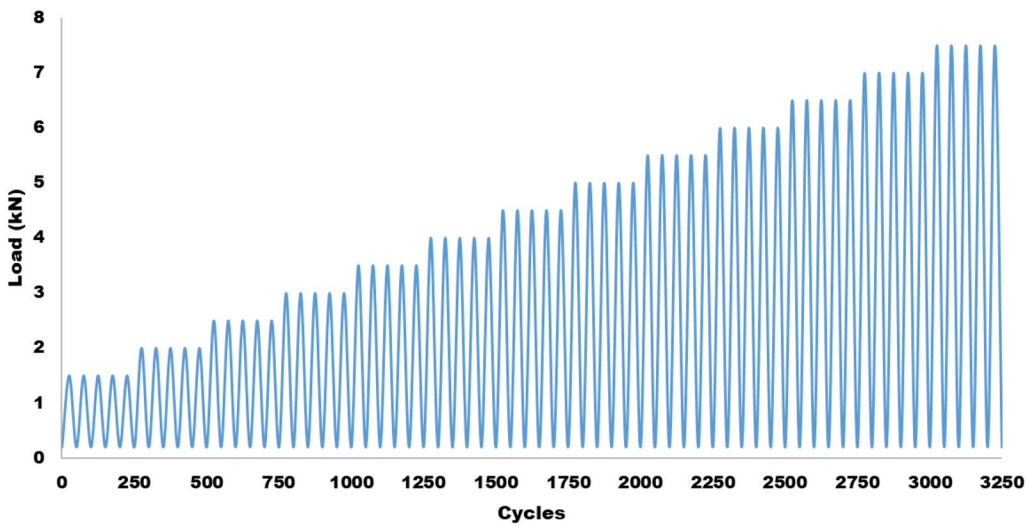


**Fig. 4** Graphical representation of the loading history (load versus the number of cycles).

the loading instrument. Fig. 4 shows the graphical representation of the loading history. The maximum load was increased as the loading cycle increased.

Table 4 describes the maximum loads from the fatigue test and the results from the AE test at failure. Based on the results, the summation of the total number of cycles, which leads to failure, decreased as the notch-to-depth ratio increased. Type I beam recorded the highest number of cycles of load that leads to failure as it had the lowest notch-to-depth ratio. Such observation was due to the increment in the notch-to-depth ratio, which in turn decrease the cement matrix bond. The reduced bond between the aggregate and cement mortar was attributed to a weaker beam, consequently failing the specimen even with a small failure load (Sagar et al., 2012).

The number of AE events decreased with the increasing notch-to-depth ratio. The number of cycles that leads to failure was able to influence the acquired AE activity (Sagar et al., 2012). The increment of AE event as the decrease of the notch-to-depth ratio implied that beams with the short height of notch depth was more brittle and exhibited a higher number of micro-crack formation before the final failure compared to beams with higher ratio of height notch-to-depth length. The number of AE events increased rapidly as the specimen approached the fatigue failure, signifying that the AE event parameter was a vital indicator of the total failure.

Additionally, the AE technique possesses the advantage of monitoring the damage in real-time, which make AE a beneficial tool to locate and identify fatigue crack growth throughout the testing. Note that the fatigue crack in quasi-brittle materials, such as concrete, is difficult to be observed and measured because the crack is hardly visible until a specific number of cycles that promoted the crack was attained. This phenomenon, which occurred during the critical stage, was very close to failure as the materials had a catastrophic failure (Shahidan et al., 2012).

A specimen at the critical stage requires only a few seconds to fail. The available AE parameters, such as events, counts, hits, signal strength, and absolute energy represent the critical stage of the specimens and provides an early warning as the specimen approaches failure. Hence, the AE parameters can be suitably used to predict the failure of quasi-brittle materials.

Acquisition and analysis of AE activities that exceed the prescribed threshold value. The interaction display graph illustrates the three distinct stages of fatigue failure, namely the first stage, the second stage, and the third stage. The number of AE events appears to decrease as the notch-to-depth ratio increases. This is because the ligament size increases as the notch-to-depth ratio of the samples increases. Nevertheless, when the density of AE-events is considered, the Type IV beam has a lower AE-event location density than the Type I beam. This indicates that the material with a short ligament length is more fragile and requires fewer micro-cracks to fail than the specimen with a long ligament length.

Furthermore, the cumulative AE hits, cumulative AE signal strength, cumulative AE absolute energy, and cumulative AE amplitude increased rapidly when the crack was initiated in the crack propagation stage. The increment of the cumulative values of the AE parameter was the smallest in the stable cracking stage (Yu et al., 2013). The highest slope of the curve was recorded when the crack was approaching failure. Fig. 5b shows the sudden increment in the absolute energy at the last stage of the fatigue failure mechanism. The cumulative values of the AE parameter increased dramatically during the unstable cracking stage, leading to the fracture process of the specimens (Yu et al., 2013).

Fig. 5 shows the results of the activity display for Type I, II, III, and IV beams. At the beginning of the test, the AE parameter values increased in small amplitude, suggesting the formation of weak regions and the initiation of flaws, which was present in the first stage of the fatigue failure mechanism., The absolute energy values increased constantly as the load was increased until the occurrence of the second stage of the fatigue failure mechanism, which was indicated by the sudden increment in the activity display. The concrete was in the second stage of the fatigue failure mechanism when the number of loading cycles required to initiate a fatigue crack and to propagate the crack was sufficient. Once the loading cycles were adequate to initiate the micro-crack, the values of

**Table 4** AE data parameter for different types of notched beam.

| Notch/depth ratio | Peak load (kN) | Number of AE events | Number of AE counts | Number of AE hits | AE energy | Number of cycles at failure |
|---|---|---|---|---|---|---|
| 0.15 | 16.5 | 8252 | 31,447,988 | 571,746 | 50,508,338 | 7555 |
| 0.25 | 11.0 | 7461 | 817,532 | 31,323 | 1,357,883 | 5000 |
| 0.35 | 8.0 | 1230 | 720,360 | 23,840 | 1,935,340 | 3334 |
| 0.45 | 6.0 | 1739 | 579,035 | 53,297 | 1,462,184 | 2277 |

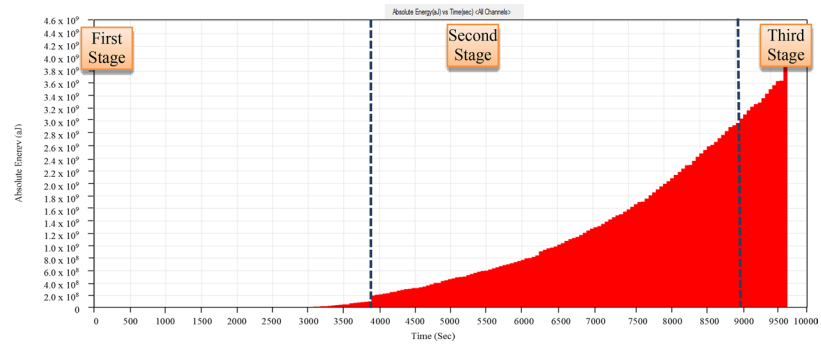


**(a)**

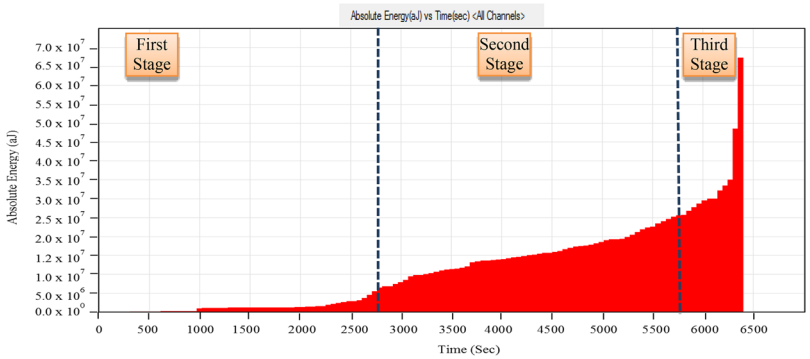


**(b)**

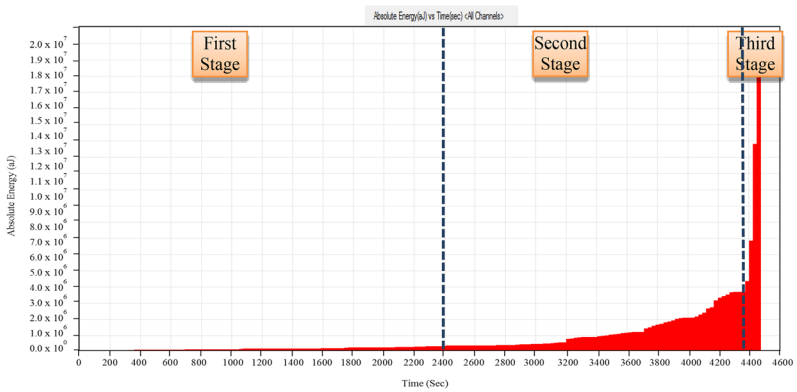


**(c)**

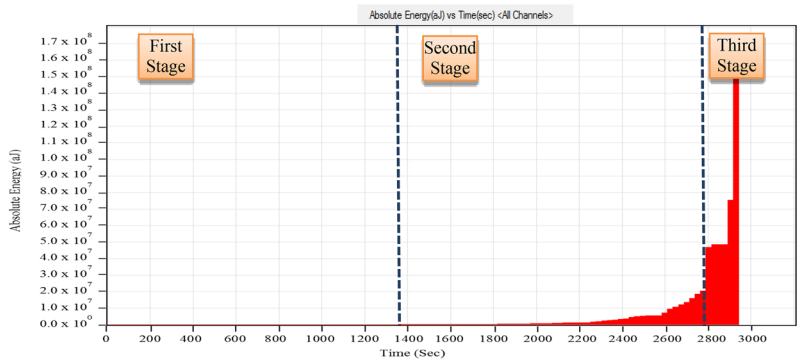


**(d)**

**Fig. 5** The AE absolute energy of (**a**) Type I beam, (**b**) Type II beam (**c**) Type III beam, (**d**) Type IV beam.

AE parameters increased and the initial flaws began to progressively grow into critical size.

As the cyclic loading continues, the growth of the dominant micro-cracks continued until the remaining un-cracked area of the specimen was unable to sustain the increment of the cyclic load. Once the fracture toughness of the specimen tested was exceeded, the remaining cross-section of the beam experienced a rapid fracture. This rapid overload fracture was described as the third stage of the fatigue failure mechanism. The higher increment of AE energy was due to the development of unstable rapid propagation of macro-cracks that led to the specimen failure. Fig. 6 demonstrates the failure specimen after the test was completed.

### 4.3 b-value Analysis

The b-value analysis was carried out to classify the damage of the plain concrete specimen. The b-value was determined from the slope of a log-linear plot of the number of hits at a higher amplitude versus amplitude in dB (Pollock, 1981). The *b*-value was an effective parameter related to the stages of fracture due to the magnitude of fracture, which was associated with the AE amplitude (Shahidan et al., 2012). Since each failure mechanism exhibit a unique b-value (Carey, 1991; Pollock, 1981), therefore, the b-value varied during the test. The AE data were divided according to the stage of loading. The maximum load was increased by 0.5 kN for each stage. Meanwhile, the number of cycles of stages depended on the failure load for each type of specimen's notch-to-depth ratio. The b-value analysis was carried out for 500 hits for each stage.

Fig. 7a illustrates the *b*-value data for the Type I beam. The analysis of the *b*-value began at load stage 7 due to the insufficient AE hits recorded from load stage 1 to 6. This was in agreement with the condition of the specimen in which the micro-crack and macro-crack did not develop on the surface of the specimen in the earlier stages of loading, particularly from load stages 1 to 6 for this type of beam. Initially, the b-value decreased at cycles 5500 and was followed by an almost constant b-value after cycles 5750 before finally recording a sudden drop in the last phase. The emitted AE hits during the early stages of cyclic loading were due to the small opening and closing of the available micro-cracks. As the cyclic loading stages increased, the *b*-value also increased and achieved a constant phase. In this stage, many micro-cracks started to develop, as can be proven by the increasing AE absolute energy and cumulative AE signal strength. In the last stage, the rapid propagation of a major crack took place, leading to the specimen's failure. It was observed from the *b*-value graph that a sudden decrease in the *b*-value corresponded to the total failure and complete fracture in the ligament.

A similar pattern was observed for Type II, Type III, and Type IV beams, respectively, as shown in Fig. 7b–d, whereby no significant AE hits were recorded in the early stages. Type III and IV beams only exhibited the last phase of the fatigue failure mechanism, where a sudden drop of b-value occurred. This was due to the high notch-to-depth ratio of these beams that were unable to display the real pattern of the b-value when the concrete withstand the fatigue cyclic load.

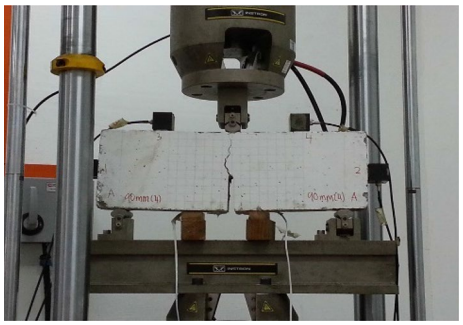

**Fig. 6** Failure of the specimen after undergoing fatigue loading.

### 4.4 The Ib-value Analysis

The primary parameters used in the calculation of the Ib-value include the mean of amplitude and standard deviation from a set of amplitude data for each stage. The Ib-value analysis was carried for a set of 500 hits, which was similar to that of the b-value analysis. Prior to the Ib-value analysis, a test trial was performed for a different set of total hits numbers and a set of 500 hits that showed better results and obeyed the Ib-value specification. For every 500 cycles, a 0.5 kN increase in the maximum load is induced by the fatigue loading. The Ib-value analysis was performed against the number of cycles to provide the damage severity information throughout the increasing of maximum load for each of the stages and cycles of the cyclic load.

Fig. 8a depicts the Ib-value analysis for the Type I beam, which began at load stage 7. The results showed similar patterns to those obtained from the b-value analysis. Nevertheless, the distribution in the Ib-value analysis was more visible and showed a distinct distribution of the three important stages of the fatigue failure mechanism. The early stage of loading recorded a drop in the Ib-value, beginning at load stage 8. At load stage 9, the computed Ib-value was 3.6524, which dropped until 1.1620 at loading stage 10. This indicated that the generated AE was due to the small opening in the crack mouth of micro-cracks, where frictional energy dissipation from the rubbing of fine and coarse aggregate particles of the concrete

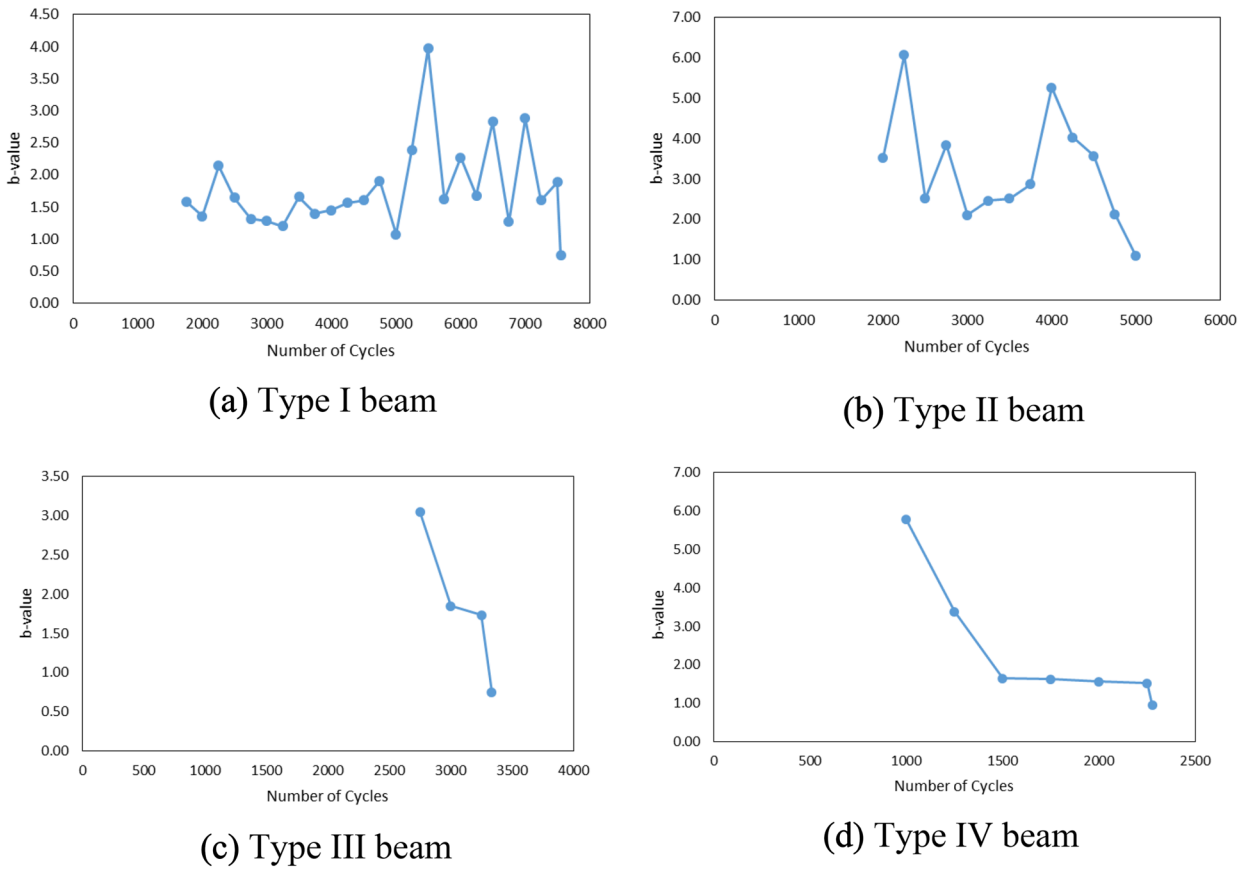


**Fig. 7** The *b*-value versus the number of cycles.

right on the notch zone took place. This was followed by a constant Ib-value before ending with a sudden drop of the Ib-value at the load stage of 28 until the load stage of 31. The constant phase of Ib-value started at load stage 14 and ended at load stage 27 in which rapid growth of micro-cracks occurred during this phase. The Ib-value at this phase was between 1.06 and 2.33.

The final stage of the fatigue failure mechanism took place when a sudden drop in Ib-value was recorded. This phase indicated the rapid and unstable growth of micro-cracks to macro-cracks. The AE energy was also released by the formation of the complete fracture zone and unstable crack propagation that led to a total failure. The transition from the second to the final stage recorded a significant finding in which the critical stage of damage was identified and provided early warnings of emerging failures. The emerging failure was predicted at the point when the Ib-value started to drop.

Fig. 8b exhibits the three stages of fatigue failure mechanism for Type II beam. A decrease in the Ib-value firstly occurred at load stage 9, followed by a constant phase of the Ib-value at load stage 10 and ended at load stage 15. A failure phase occurred at stage 16 when the Ib-value dropped sharply until the final stage, which was at load stage 20. In contrast, Fig. 8c shows that the Ib-value for beam Type III began at load stage 11 with the maximum load of 6.5 kN, which recorded a similar pattern to beam Type IV, as shown in Fig. 8d. The failure of the Ib-value recorded for Type II, Type III, and Type IV beams were 0.9440, 0.9630, and 0.9700, respectively. In addition, there was no clear correlation between Type III and Type IV and the Ib-value analysis due to the high notch-to-depth ratio. On the contrary, the Ib-values of Type I and Type II beams showed a better correlation between the degrees of localisation of damage. Previously, a study performed by Proverbio et al. (2009) showed that the Ib-value recorded better results in evaluating the damage conditions of concrete structures.

### 4.5 Severity Analysis

The severity analysis was performed for a set of 500 AE hits, which was similar to that of the *b*-value and Ib-value. The variation of the damage severity was carried out for each stage of each type of beam. It was found

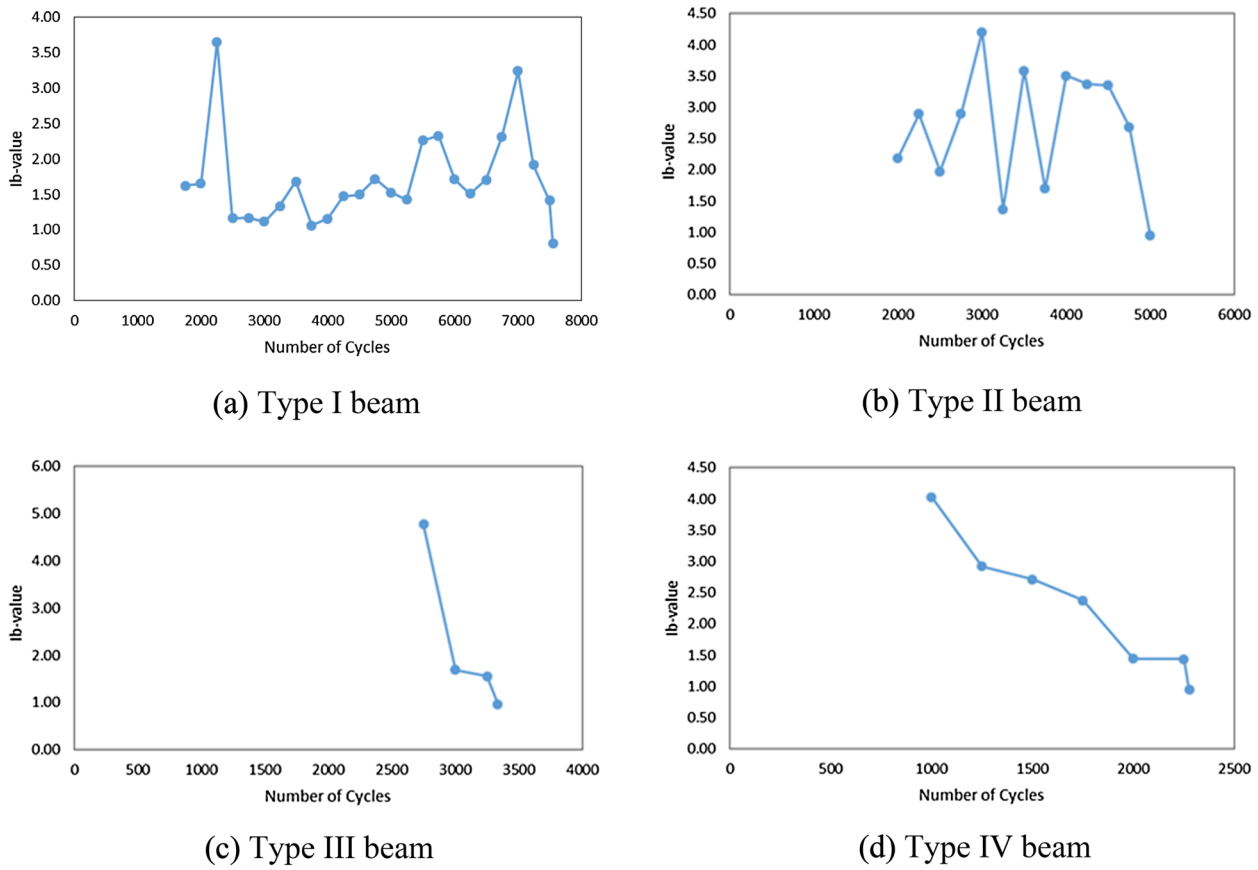


**Fig. 8** The Ib-value versus the number of cycles.

that the number of cycles corresponded to the stage of increment load applied. The graph of severity against the number of cycles for all four types of beam is shown in Fig. 9a–d. In the last stage of the increment of cyclic loading, a sudden and substantial increase in severity occurred for all types of beams. The high severity during failure was also observed in past studies (Shahidan et al., 2012), which reflected the occurrence of higher damage that leads to the specimen failure. Notably, the severity index observed for Type II beam during load stage 19 was equal to 14.86, while at the last load stage, a sudden failure occurred with the value of severity index recorded at 2315.04. The results obtained from the severity analysis proved that the failure pattern of the concrete undergoing fatigue cyclic load was a catastrophic failure (Antonaci et al., 2012; Rteil, 2007; Shahidan et al., 2012).

Fig. 10 demonstrates the variation of severity against the number of cyclic loads as the maximum load was increased for each stage. The highest severity value computed at the failure was recorded by the Type I beam, indicating that the Type I beam experienced severe damage at the failure stage compared to the Type II beam, Type III beam and Type IV beam.

### 4.6 Intensity Analysis

The intensity analysis was employed to evaluate the level of deterioration of the concrete structure by computing two main parameters comprising HI and $S_r$. Fig. 11a–d summarise the intensity data for Type I, Type II, Type III, and Type IV beam, respectively. The damage was classified into five levels, namely, level A, level B, level C, level D, and level E. The details of each level are described in Table 2. Based on Fig. 11, the intensity value for earlier stages of the load was plotted at the lower area of the intensity chart, which was at level C, while the intensity value computed during the failure stage was located at the upper area of the intensity chart, which was at level E. Thus, the intensity chart pattern obtained when the cyclic load was applied on the concrete specimen recorded a higher intensity value at the upper level of the intensity chart, while a lower intensity value was recorded at the lower level of the intensity chart. The low intensity was associated with earlier stages of cyclic load.

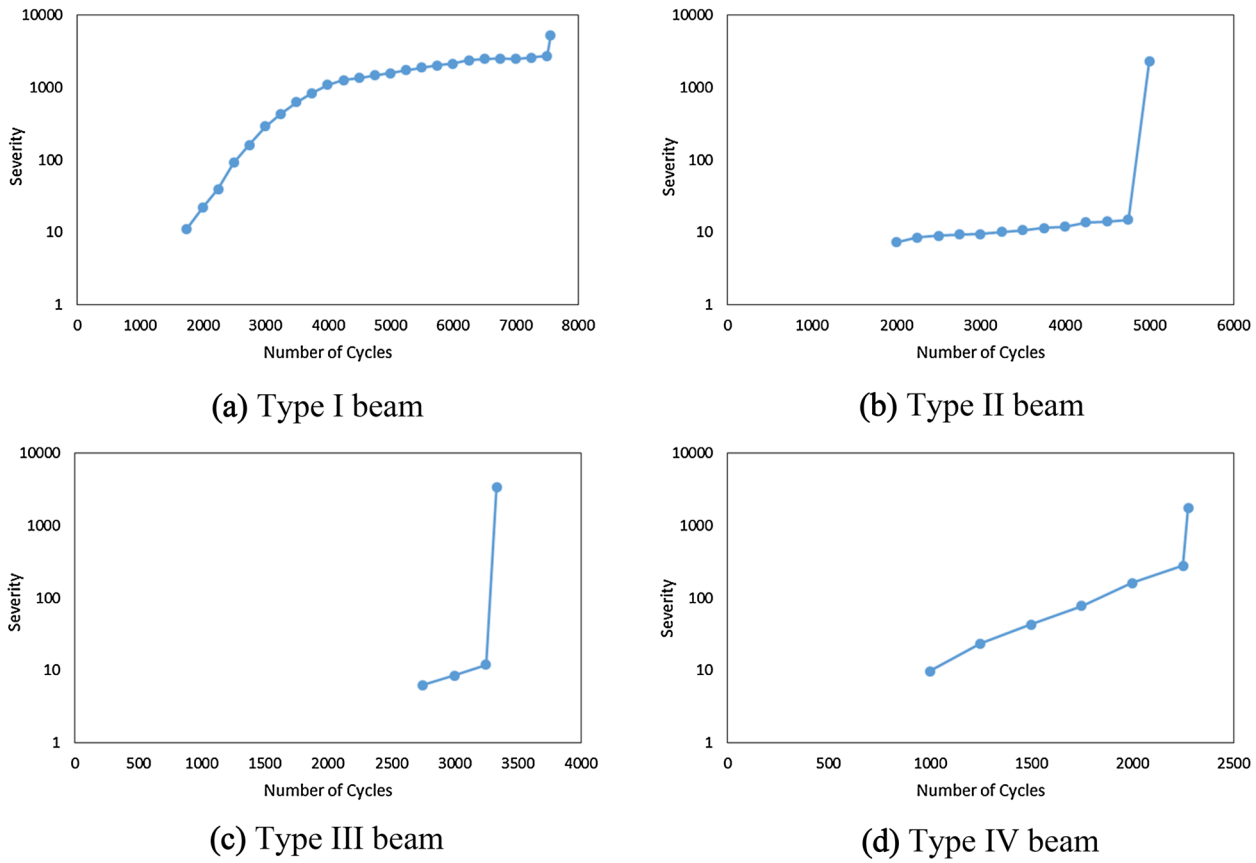


**Fig. 9** Severity versus the number of cycles.

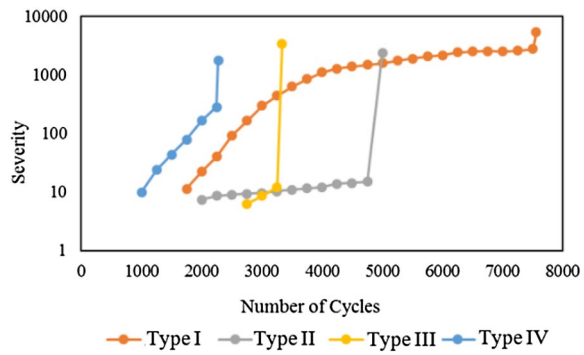


**Fig. 10** Variation of the severity against the number of cycles for all types of beams.

Briefly, there were no data recorded at level A and level B in this case. At level C, the damage was classified as minor damage. Load stages 7, 8, and 9 were located at level C in the intensity chart. As the load increased, the level of damage shifted from level C to level D. Load stages 10, 11, 12, and 13 were located at level D. The damage at level D was classified as the major damage in which the micro-cracks started to transform into macro-cracks, while the existing cracks from level C started to localise. The severity increased gradually as the load stage increased. The other stages, which started from load stage 14 until the failure stage at load stage 31, were scattered at level E of the intensity chart. At level E, the existing crack was more localised as the crack length increased, which was visibly observed near the last stage. At this level, the number of micro-cracks developed increased as the AE signal strength and AE energy increased. The number of micro-cracks that transformed into macro-cracks also increased as the AE parameters gradually increased. The failure stage occurred at load stage 31 with the highest severity recorded among the other stages.

## 5 Conclusion

The application of the AE technique was efficient in measuring the damage mechanism assessment, allowing for easy classification of the structure's degree of damage level. The AE analyses, which included the

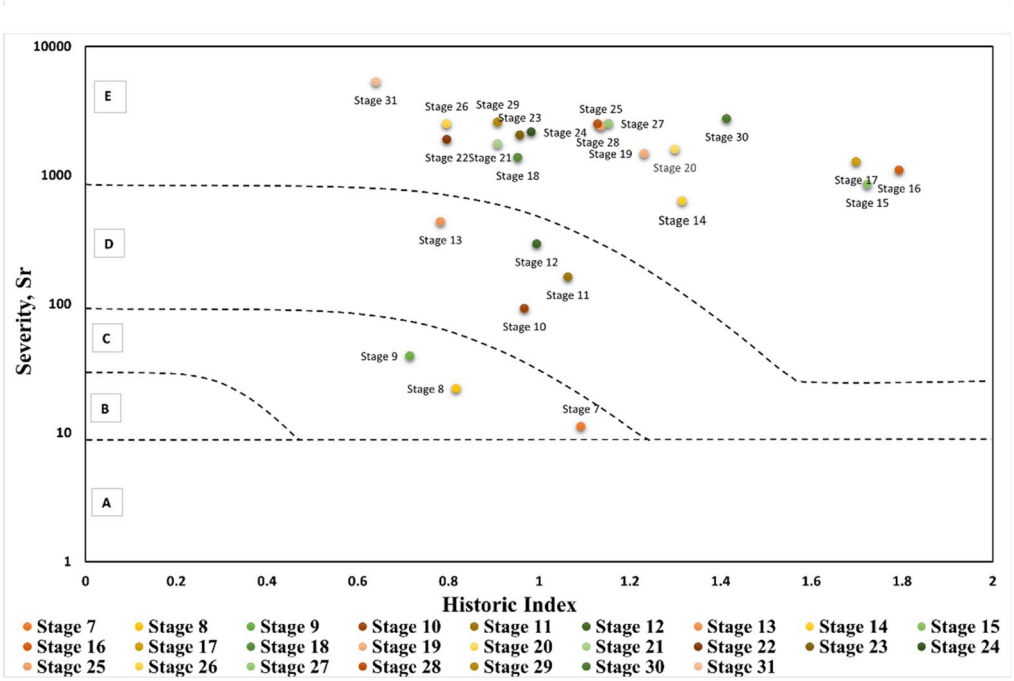


(a) Type I beam

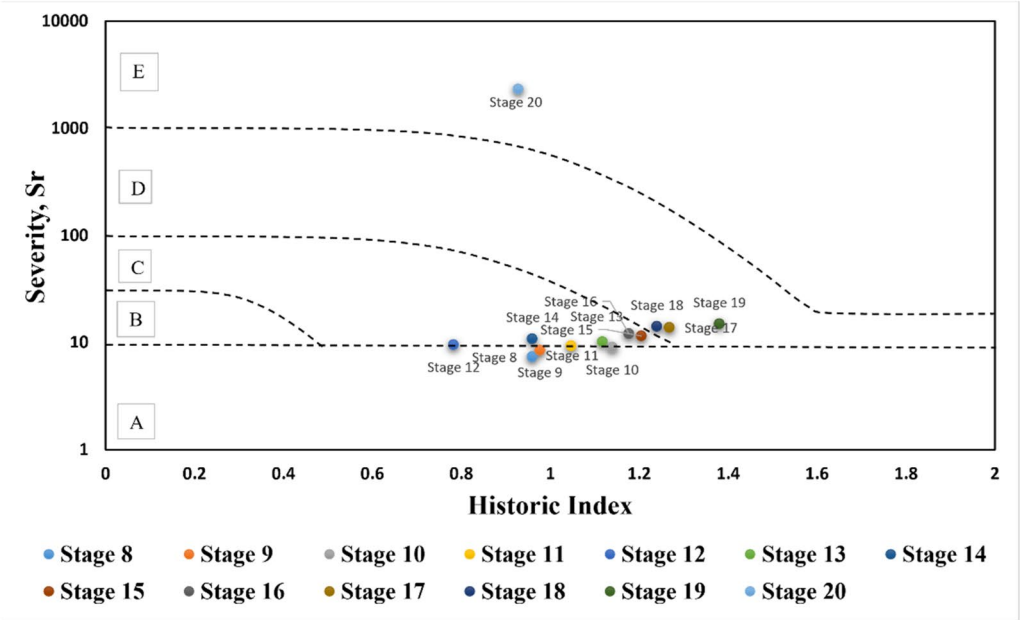


(b) Type II beam

**Fig. 11** Intensity analysis.

*b*-value, Ib-value, intensity evaluation, and severity analysis, were able to quantify the occurrence of fatigue-induced damage levels. Additionally, the use of AE enables the determination of the structure's stability or instability condition. Furthermore, AE provided the advantage of forecasting the extent of structural

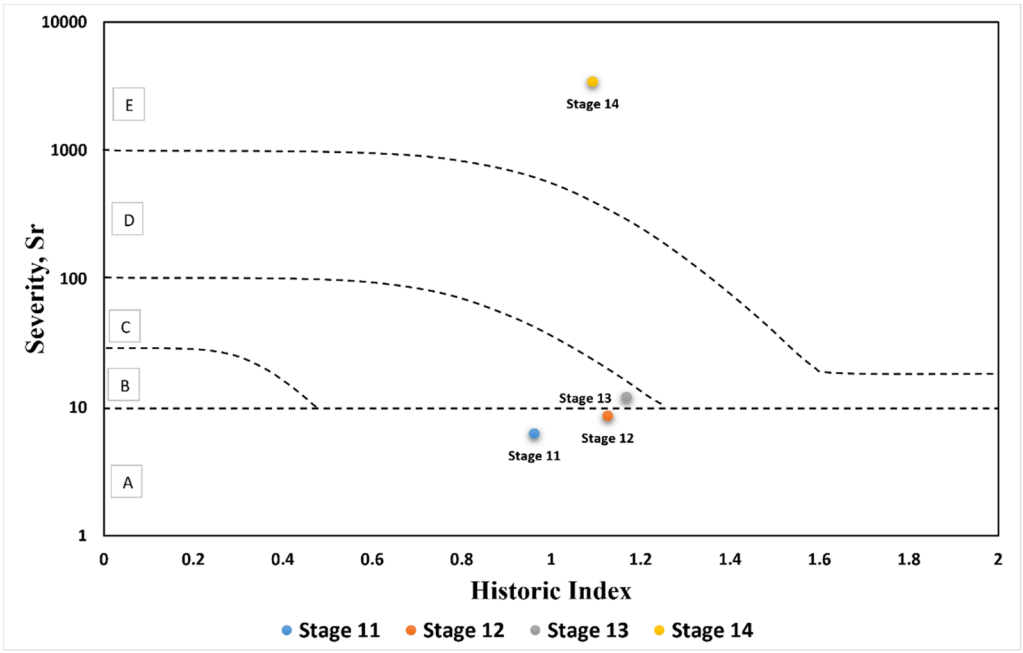


(c) Type III beam

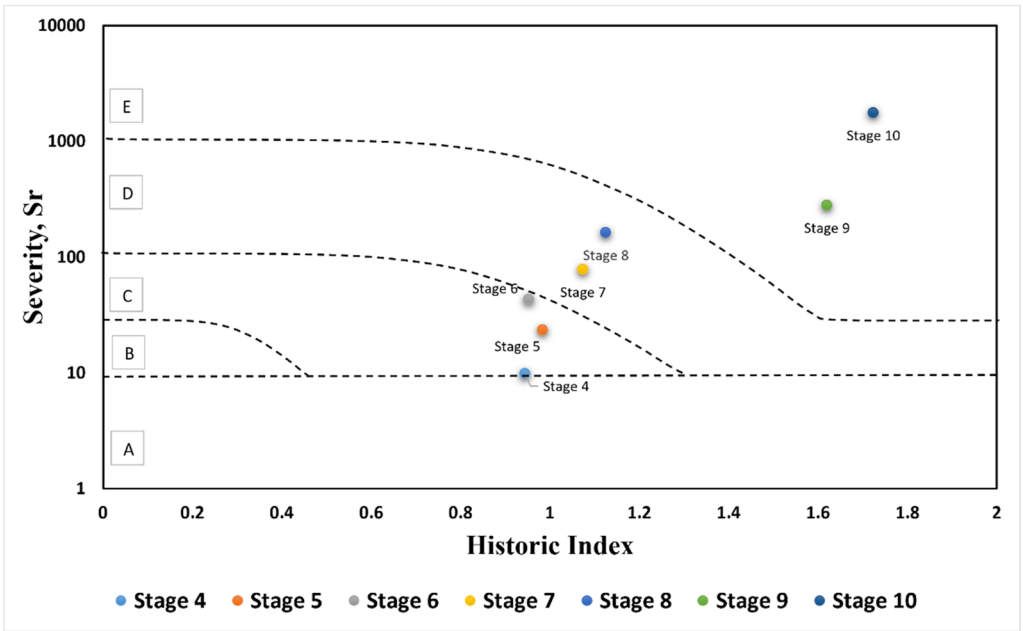


(d) Type IV beam

**Fig. 11** continued

damage based on the AE parameters obtained during monitoring, ensuring advanced warning in the event of malfunction. All analyses used AE parameters as indicators for evaluating fatigue damage. In summary, the following conclusions were drawn considering the study's objectives:

- Initial deceleration of crack growth is followed by accelerated growth until failure.

- Using the acoustic emission procedure, the number of AE-events, AE-counts, AE-hits, and AE-energy can be used to calculate the extent of cracking and damage that occurs during fatigue loading. The number of AE-events is a key predictor of fatigue crack growth and failure, as the events rise significantly toward incipient fatigue failure.
- The Ib-value results allowed for the differentiation of the fatigue failure mechanism's stages. Besides, the Ib-value analysis produced more accurate results than the *b*-value analysis in aspects of classifying the fatigue damage mechanism. Fatigue crack growth can be tracked using AE signal analysis techniques such as *b*-value and Ib-value calculations. This measure makes it simple to determine the onset of unstable crack propagation. This would aid in fatigue test control, preventing the test specimen from failing unexpectedly.
- The severity analysis revealed that as loading cycles increased, the severity increased until failure occurred.
- An analysis of the intensity chart indicates that the high-intensity values were plotted at the top, while the low-intensity values were plotted at the bottom. As the specimen approached failure, the severity value range increased. Using intensity analysis, the extent of the damage generated during fatigue loading could be classified. The severity was lowest during the initial stages of cyclic loading and increased until failure occurred. The failure stage had the highest severity value. This study has therefore demonstrated that the intensity analysis approach can be used to quantify damage in concrete structures.

**Acknowledgements**
The authors would like to express their gratitude to the Ministry of Higher Education Malaysia and Universiti Teknologi MARA, Shah Alam and Universiti Sains Malaysia for supporting this publication via research grant RACER/1/2019/TK01/UITM/2.

**Authors' contributions**
All authors have contributed to work and wrote the paper. The authors confirm contribution to the paper as follows: study conception and design: SAK, NMB. Data collection: SAK. Analysis and interpretation of results: SAK, AJ. Writing—original draft: SAK. Writing—review and edit: NKM. All authors read and approved the final manuscript.

**Author's Information**
Sakhiah Abdul Kudus is Senior Lecturer at School of Civil Engineering, College of Engineering, Universiti Teknologi MARA Shah Alam, Malaysia and Associate Fellow at Institute for Infrastructure Engineering and Sustainable Management (IIESM), Universiti Technologi MARA Shah Alam, Malaysia. Norazura Muhamad Bunnori is Associate Professor at Department of Civil Engineering, Faculty of Engineering University of Malaya, Kuala Lumpur, Malaysia. Nur Kamaliah Mustaffa is Senior Lecturer at School of Civil Engineering, College of Engineering, Universiti Teknologi MARA Shah Alam, Malaysia. Adiza Jamadin is Senior Lecturer at School of Civil Engineering, College of Engineering, Universiti Teknologi MARA Shah Alam, Malaysia and Associate Fellow at Institute for Infrastructure Engineering and Sustainable Management (IIESM), Universiti Technologi MARA Shah Alam, Malaysia.

**Funding**
This research was supported by a Grant RACER/1/2019/TK01/UITM/2 Ministry of Higher Education Malaysia.

**Availability of data and materials**
Not applicable.

## Declarations

**Competing interests**
The authors declared that they have no competing interests.

**Author details**
[1]School of Civil Engineering, College of Engineering, Universiti Teknologi MARA, 40450 Shah Alam, Selangor, Malaysia. [2]Institute for Infrastructure Engineering and Sustainable Management (IIESM), Universiti Teknologi MARA, 40450 Shah Alam, Malaysia. [3]Department of Civil Engineering, Faculty of Engineering, University of Malaya, 50603 Kuala Lumpur, , Malaysia.

Received: 6 November 2021 Accepted: 9 March 2022
Published online: 09 June 2022

**References**

Aggelis, D. G. (2011). Classification of cracking mode in concrete by acoustic emission parameters. *Mechanics Research Communications, 38*(3), 153–157.

Angelis, T. G., Shiotani, T., Momoki, S., & Hirama, A. (2009). Acoustic emission and ultrasound for damage characterization of concrete elements. *ACI Materials Journal, 106*(6), 1–6.

Antonaci, P., Bocca, P., & Masera, D. (2012). Fatigue crack propagation monitoring by Acoustic Emission signal analysis. *Engineering Fracture Mechanics, 81*, 26–32.

American Society for Testing and Material. (2006). ASTM E 2478:2006. Standard practice for determining damage-based design stress for fiberglass reinforced plastic (FRP) materials using acoustic emission. West 203 Conshohocken, Pennsylvania: ASTM International, p. 6.

Baqersad, J., Niezrecki, C., & Avitabile, P. (2015). Full-field dynamic strain prediction on a wind turbine using displacements of optical targets measured by stereophotogrammetry. *Mechanical Systems and Signal Processing, 62*, 284–295.

Basri, S. R., Bunnori, N. M., Kudus, S. A., Shahiron, S., Jamil, M. N. M., & Noorsuhada, M. N. (2013). Applications of acoustic emission technique associated with the fracture process zone in concrete beam—A review. *Advanced Materials Research. Trans Tech Publication., 626*, 147–151.

Bruck, H. A., McNeill, S. R., Sutton, M. A., & Peters, W. H. (1989). Digital image correlation using Newton-Raphson method of partial differential correction. *Experimental Mechanics, 29*(3), 261–267.

Bunnori, M. N. (2008). Acoustic emission technique for the Damag assessment of reinforced concrete structures. Ph.D Thesis, Cardiff University, Wales, UK.

Bunnori, N., Nor, N., Jiun, K., & Kudus, S. (2016). Analysis of failure mechanisms in fatigue test of reinforced concrete beam utilizing acoustic emission. The International Journal of Multiphysics, 8(4).

Bunnori, M. N., Lark, R. J., & Holford, K. M. (2011). The use of acoustic emission for the early detection of cracking in concrete structures. *Magazine of Concrete Research, 63*(9), 683–688.

Carey S. (1991). Damage detection and characterization in CFRP composites using acoustic emission and acousto-ultrasonics. Ph.D Thesis, University of South Carolina.

Carpinteri, A., Lacidogna, G., Corrado, M., & Di Battista, E. (2016). Cracking and crackling in concrete-like materials: A dynamic energy balance. *Engineering Fracture Mechanics, 155*, 130–144.

Carpinteri, A., Lacidogna, G., & Niccolini, G. (2009). Fractal analysis of damage detected in concrete structural elements under loading. *Chaos, Solitons & Fractals, 42*(4), 2047–2056.

Chotickai, P. (2001). Acoustic emission monitoring of prestressed bridge girders with premature concrete deterioration. M.Sc Thesis, University of Texas, Austin.

Colombo, I. S., Main, I. G., & Forde, M. C. (2003). Assessing damage of reinforced concrete beam using "b-value" analysis of acoustic emission signals. *Journal of Materials in Civil Engineering, 15*(3), 280–286.

Croxford, A. J., Wilcox, P. D., Drinkwater, B. W., & Konstantinidis, G. (2007). Strategies for guided-wave structural health monitoring. *Proceedings of the Royal Society a: Mathematical, Physical and Engineering Sciences, 463*(2087), 2961–2981.

Degala S. (2008). Acoustic emission monitoring of reinforced concrete systems retrofitted with CFRP [Master's Thesis]. University of Pittsburgh.

Degala, S., Rizzo, P., Ramanathan, K., & Harries, K. A. (2009). Acoustic emission monitoring of CFRP reinforced concrete slabs. *Construction and Building Materials, 23*(5), 2016–2026.

Eskandari, H., Muralidhara, S., Raghuprasad, B. K., & Reddy, B. V. V. (2010). Size effect in self consolidating concrete beams with and without notches. *Sadhana, 35*, 303–317.

Farrar, C. R., & Worden, K. (2012). *Structural health monitoring: A machine learning perspective*. Wiley.

Finlayson, R. D., Firesel, M., Carlos, M., Cole, P., & Lenain, J. C. (2001). Health monitoring of aerospace structures with acoustic emission and acousto-ultrasonics. *Insight, 43*(3), 1–4.

Glišić, B., & Inaudi, D. (2007). *Fibre optic methods for structural health monitoring* (p. 276). Wiley.

Golaski, L., Pawel, G., & Kanji, O. (2002). Diagnostic of reinforced concrete bridge by acoustic emission. *Journal of Acoustic Emission, 20*(1), 83–98.

Gostautas, R. S., Ramirez, G., Peterman, R. J., & Meggers, D. (2005). Acoustic emission monitoring and analysis of glass fiber-reinforced composites bridge decks. *Journal of Bridge Engineering, 10*(6), 713–721.

Holford, K. M., Davies, A. W., Pullin, R., & Carter, D. C. (2001). Damage location in steel bridges by acoustic emission. *Journal of Intelligent Material Systems and Structures, 12*(8), 567–576.

Im, S. B., Hurlebaus, S., & Kang, Y. J. (2013). Summary review of GPS technology for structural health monitoring. *Journal of Structural Engineering, 139*(10), 1653–1664.

Kaphle, M., Tan A. C. C., Thambiratnam, D. P., & Chan, T. H. T. (2011). Damage Quantification Techniques in Acoustic Emission Monitoring. WCEAM 2011 Sixth World Congress on Engineering Asset Management, Cincinnati, OH, USA, p. 1–6.

Karihaloo, B. L. (1995). Fracture mechanics and structural concrete, Longman Scientific & Technical, England.

Kim, S., Pakzad, S., Culler, D., Demmel, J., Fenves, G., Glaser, S., & Turon, M. (2006). Wireless sensor networks for structural health monitoring. In *Proceedings of the 4th international conference on Embedded networked sensor systems* (pp. 427–428).

Kudus, S. A. (2014). Study on fatigue damage of concrete beams with variable notched depth using acoustic emission technique (Doctoral dissertation, Universiti Sains Malaysia).

Kurz, J. H., Finck, F., Grosse, C. U., & Reinhardt, H. W. (2006). Stress drop and stress distribution in concrete quantified over time by the b-value analysis. *Structural Health Monitoring, 5*(1), 69–81.

Lacidogna, G., Piana, G., Accornero, F., & Carpinteri, A. (2020). Multi-technique damage monitoring of concrete beams: acoustic emission, digital image correlation, dynamic identification. *Construction and Building Materials, 242*, 118114.

López-Higuera, J. M., Cobo, L. R., Incera, A. Q., & Cobo, A. (2011). Fiber optic sensors in structural health monitoring. *Journal of Lightwave Technology, 29*(4), 587–608.

Lovejoy, S. C. (2008). Acoustic emission testing of beams to simulate SHM of vintage reinforced concrete deck girder highway bridges. *Structural Health Monitoring, 7*(4), 329.

Lynch, J. P. (2007). An overview of wireless structural health monitoring for civil structures. *Philosophical Transactions of the Royal Society a: Mathematical, Physical and Engineering Sciences, 365*(1851), 345–372.

Lynch, J. P., & Loh, K. J. (2006). A summary review of wireless sensors and sensor networks for structural health monitoring. *Shock and Vibration Digest, 38*(2), 91–130.

Mitra, M., & Gopalakrishnan, S. (2016). Guided wave based structural health monitoring: A review. *Smart Materials and Structures, 25*(5), 053001.

Nagayama, T., & Spencer, B. F., Jr. (2007). *Structural health monitoring using smart sensors*. University of Illinois at Urbana-Champaign.

Nair, A., & Cai, C. S. (2010). Acoustic emission monitoring of bridges: Review and case studies. *Engineering Structures, 32*(6), 1704–1714.

Ohno, K., & Ohtsu, M. (2010). Crack classification in concrete based on acoustic emission. *Construction and Building Materials, 24*(12), 2339–2346.

Pollock, A. A. (1981). Acoustic emission amplitude distributions. *International Advances in Nondestructive Testing, 7*, 215–239.

Prashanth, M. H., Singh, P., & Kishen, J. C. (2019). Role of longitudinal reinforcement on the behavior of under reinforced concrete beams subjected to fatigue loading. *International Journal of Fatigue, 125*, 271–290.

Proverbio, E., Venturi, V. & Campanella, G. (2009). Damage assessment in post-tensioned concrete viaduct by b- and Ib- value analysis of AE signal. Proceeding Non-Destructive Testing in Civil Engineering. 30 June–3 July, Nantes, France.

Proverbio, E. (2011). Evaluation of deterioration in reinforced concrete structures by AE technique. *Materials and Corrosion, 62*, 161–169.

Raghavan, A. (2007). Guided-wave structural health monitoring (Doctoral dissertation).

Rao, M. V. M. S., & Lakshmi, K. J. P. (2005). Analysis of b-value and improved b-value of acoustic emissions accompanying rock fracture. *Current Science, 89*, 1577–1582.

RILEM. (1991). TC 89-FMT Fracture mechanics of concrete–test methods. *Materials and Structures, 23*, 461–465.

Rteil, A. (2007). Fatigue Bond Behaviour of Corroded Reinforcement and CFRP Confined Concrete. Ph.D Thesis University of Waterloo, Waterloo, Ontario, Canada.

Sagar, R. V., Prasad, B. K. R., & Kumar, S. S. (2012). An experimental study on cracking evolution in concrete and cement mortar by the b-value analysis of acoustic emission technique. *Cement and Concrete Research, 42*(8), 1094–1104.

Shah, S. G., & Chandra Kishen, J. M. (2010). Fracture behavior of concrete–concrete interface using acoustic emission technique. *Engineering Fracture Mechanics, 77*(6), 908–924.

Shahidan, S., Muhamad Bunnori, N., Md Nor, N. & Basri, S. R. (2012). Health index evaluation on acoustic emission signal for concrete structure by intensity analysis method. *Advanced Materials Research*, 403–408.

Shiotani, T., Shigeishi, M., & Ohtsu, M. (1999). Acoustic emission characteristics of concretepiles. *Construction and Building Materials, 13*(1), 73–85.

Worden, K., & Manson, G. (2007). The application of machine learning to structural health monitoring. *Philosophical Transactions of the Royal Society a: Mathematical, Physical and Engineering Sciences, 365*(1851), 515–537.

Yu, J., Ziehl, P., Matta, F., & Pollock, A. (2013). Acoustic emission detection of fatigue damage in cruciform welded joints. *Journal of Constructional Steel Research, 86*, 85–91.

Yuan, F. G., Zargar, S. A., Chen, Q., & Wang, S. (2020). Machine learning for structural health monitoring: challenges and opportunities. In Sensors and Smart Structures Technologies for Civil, Mechanical, and Aerospace Systems 2020 (Vol. 11379, p. 1137903). International Society for Optics and Photonics.

Yuyama, S., Li, Z. W., Yoshizawa, M., Tomokiyo, T., & Uomoto, T. (2001). Evaluation of fatigue damage in reinforced concrete slab by acoustic emission. *NDT & E International, 34*(6), 381–387.

## Publisher's Note

Springer Nature remains neutral with regard to jurisdictional claims in published maps and institutional affiliations.